Loads Model Development and Analysis for the F/A-18 Active Aeroelastic Wing Airplane

Michael J. Allen,* Andrew M. Lizotte,† Ryan P. Dibley,‡ and Robert Clarke§
NASA Dryden Flight Research Center, Edwards, California, 93523-0273, USA

The Active Aeroelastic Wing airplane was successfully flight-tested in March 2005. During phase 1 of the two-phase program, an onboard excitation system provided independent control surface movements that were used to develop a loads model for the wing structure and wing control surfaces. The resulting loads model, which was used to develop the control laws for phase 2, is described. The loads model was developed from flight data through the use of a multiple linear regression technique. The loads model input consisted of aircraft states and control surface positions, in addition to nonlinear inputs that were calculated from flight-measured parameters. The loads model output for each wing consisted of wing-root bending moment and torque, wing-fold bending moment and torque, inboard and outboard leading-edge flap hinge moment, trailing-edge flap hinge moment, and aileron hinge moment. The development of the Active Aeroelastic Wing loads model is described, and the ability of the model to predict loads during phase 2 research maneuvers is demonstrated. Results show a good match to phase 2 flight data for all loads except inboard and outboard leading-edge flap hinge moments at certain flight conditions. The average load prediction errors for all loads at all flight conditions are 9.1 percent for maximum stick-deflection rolls, 4.4 percent for 5-*g* windup turns, and 7.7 percent for 4-*g* rolling pullouts.

Nomenclature

A	=	loads model coefficient
AAW	=	Active Aeroelastic Wing
Ail	=	aileron
Ail_sq	=	square of aileron position
CONDUIT	=	control designer's unified toolbox
deg	=	degrees
Err_{sumsq}	=	sum of the squared error values
Err_{model}	=	load prediction error
HM	=	hinge moment
I	=	loads model intercept term
ILEF	=	inboard leading-edge flap
L_{meas}	=	measured load
L_{pred}	=	predicted load
N	=	number of data samples
Nz	=	normal acceleration
NzW	=	product of normal acceleration and total aircraft weight
OBES	=	onboard excitation system
OLEF	=	outboard leading-edge flap
p	=	roll rate
$\bar{q}$	=	dynamic pressure
R	=	number of inputs

* Aerospace Engineer, Flight Controls and Dynamics Branch, P.O. Box 273/MS 4840D, member.
† Aerospace Engineer, Aerostructures Branch, P.O. Box 273/MS 48202A, member.
‡ Aerospace Engineer, Flight Controls and Dynamics Branch, P.O. Box 273/MS 4840D.
§ Aerospace Engineer, Flight Controls and Dynamics Branch, P.O. Box 273/MS 4840D, senior member.

RPO = rolling pullout
Rud = rudder position
sign = signum function
Stab = stabilator position
TEF = trailing-edge flap
TEF_pos = positive trailing-edge flap
W = aircraft total weight
WFBM = wing-fold bending moment
WFTQ = wing-fold torque
WRBM = wing-root bending moment
WRTQ = wing-root torque
WUT = windup turn
X = input set
α = angle of attack
β = angle of sideslip
δ = deflection

Subscripts

C = Collective
D = Differential
i = sample index
j = input index
L = Left
R = Right

I. Introduction

THE Active Aeroelastic Wing (AAW) project was initiated in 1996 by the Air Force Research Laboratory and NASA to investigate the use of wing twist for roll control.[1] This concept was tested on a modified F/A-18 supersonic fighter aircraft (Boeing Company, St. Louis, Missouri) during the spring of 2005 (Fig. 1). Modifications to the AAW aircraft included new wing skin panels to reduce wing torsional stiffness, independent outboard leading-edge flap (OLEF) drive systems to increase control authority, and new control laws to drive the four control surfaces on each wing. The control laws provided surface position commands to the inboard leading-edge flap (ILEF), OLEF, trailing-edge flap (TEF), and aileron (Ail) of each wing. Differential stabilator deflection was not used in the research control laws so that roll due only to wing control surfaces could be studied.

Figure 1. Active Aeroelastic Wing airplane (EC04-0361-02).

A control design optimization tool called the control designer's unified toolbox (CONDUIT)[2] was used to determine research control law gains to maximize roll rate and produce desirable handling qualities while maintaining loads within limits. The CONDUIT-based multiple-objective design technique required accurate models of aircraft aerodynamics and loads to produce acceptable control law gains. Analytical models initially were used for this purpose but were found to be insufficient for control design,[3] so a series of 51 flights (phase 1 of the AAW program) were flown to gather data for the creation of improved aerodynamic and loads models. These models then were used to develop research control law gains. The second project phase, phase 2, consisted of 35 flights and was used to test the new control law gains. Data from these flights also were used to validate the aerodynamic and loads models.

Previous projects, which have successfully used loads models for a variety of purposes, guided the process presented in this report. For example, accurate loads models were required for the Advanced Fighter Technology Integration (AFTI) F-111 aircraft Maneuver Loads Control (MLC) experiment.[4] More recently, a loads model correction process that used F/A-18 flight data was performed for the AAW project.[3] Haas, Flitter, Milano, and Imber used a more complete approach to model component loads of a helicopter rotor system.[5,6,7]

The process presented in this report is similar to the research discussed in Refs. 5, 6, and 7, but it differs primarily in that the loads model development presented in this report is based on a higher number of flight maneuvers and is for a fixed-wing fighter aircraft at multiple subsonic and supersonic flight conditions. Neural networks were investigated early in the development of the AAW loads model with much success[8] but were abandoned, because the high extrapolation required of the leading-edge flap hinge moment (HM) predictions could not be easily analyzed for uncertainty. This report describes the processes that were used to generate an AAW loads model from flight data. Results that show loads model prediction errors for the AAW aircraft with new control laws also are presented.

II. Flight Test Data

Each wing of the AAW aircraft was instrumented with approximately 100 strain gage bridges. These strain gages were used to determine the hinge moments of the four control surfaces on each wing and the bending moment and torque loads at the wing-root and wing-fold locations.[9,10] Figure 2 shows the wing load measurement locations. Extensive ground tests were conducted to calibrate the output of the strain gages for load measurement. During these tests, each wing was covered with 52 load pads divided into 16 load zones that covered 60 percent of the lower wing surface. Each wing was subjected to a wide range of distributed and point loads, and the strain gage outputs were measured. The measured applied load values and resulting strain gage output data were used to develop equations to calculate wing loads from strain gage flight data.

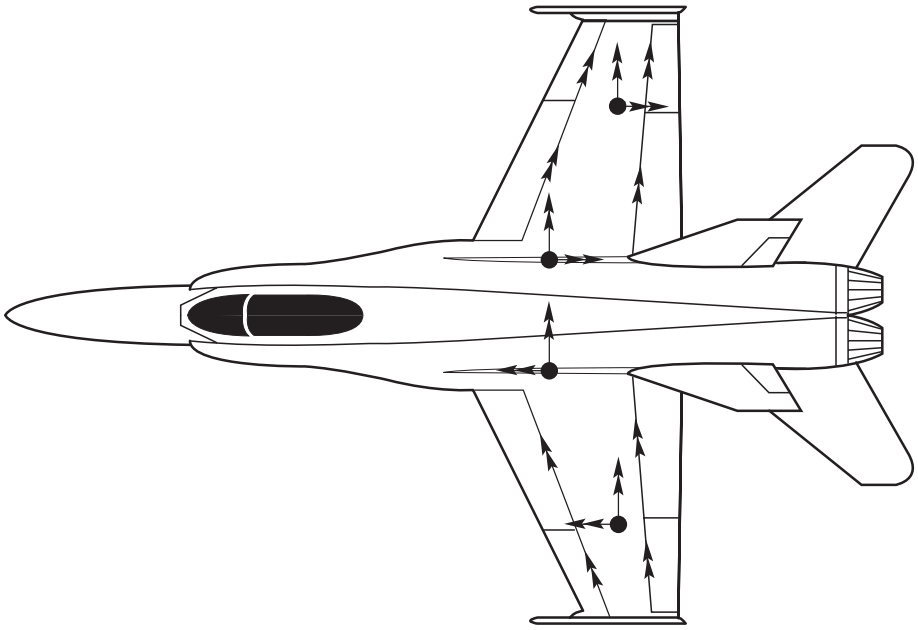

Figure 2. Locations of Active Aeroelastic Wing measured loads.

In the fall of 2002 through the spring of 2003, phase 1 flight tests of the AAW airplane were conducted to quantify wing aeroelastic effects, perform air data calibration, investigate failure scenarios, and gather data needed for the development of aerodynamic and loads models. Preprogrammed onboard excitation system (OBES) maneuvers were used to excite the aircraft response. These maneuvers consisted of a sequence of small, medium, or large collective or differential doublets individually applied to each control surface. Collective and differential doublets were used to excite the aircraft longitudinal and lateral-directional responses, respectively. Tables 1 and 2 present the input sizes for each surface doublet during each OBES maneuver. Figure 3 shows data from a large collective OBES maneuver.

Table 1. Collective onboard excitation system maneuver doublet magnitudes.

OBES size	δ_{OLEF}, deg	δ_{ILEF}, deg	δ_{TEF}, deg	δ_{OLEF} and δ_{ILEF}, deg	δ_{Ail}, deg	δ_{Stab}, deg
Small	1	1	3	1	4	0.8
Medium	2	2	4	2	5	0.8
Large	3	3	5	3	6	0.8

Table 2. Differential onboard excitation system maneuver doublet magnitudes.

OBES size	δ_{Rud}, deg	δ_{OLEF}, deg	δ_{ILEF}, deg	δ_{TEF}, deg	δ_{Ail}, deg	δ_{Stab}, deg	δ_{OLEF} and δ_{ILEF}, deg
Small	4	2	2	6	8	6	2
Medium	4	4	4	8	10	6	4
Large	4	6	6	10	12	6	6

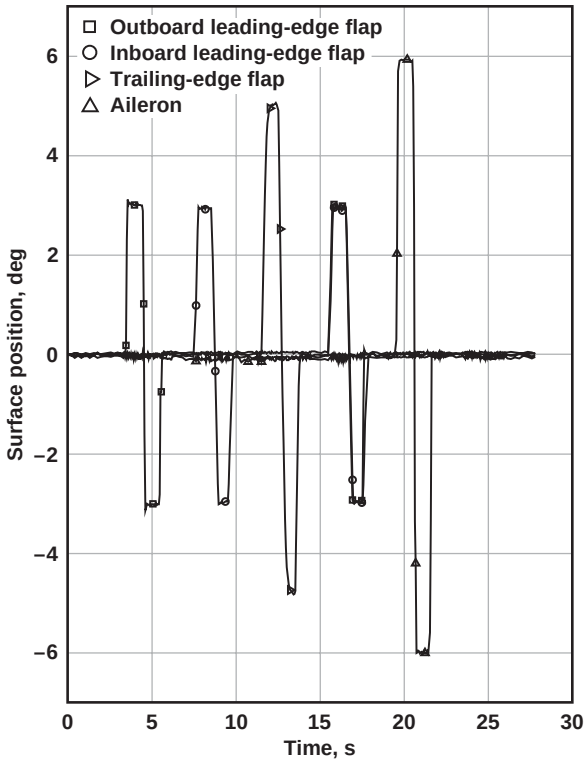

Figure 3. Large collective onboard excitation system maneuver. Stabilator position is not shown.

Because the OBES maneuvers were relatively small in magnitude, additional piloted maneuvers were flown to identify load characteristics at higher load levels. These maneuvers consisted of 5-*g* windup turns (WUTs); 4-*g* rolling pullouts (RPOs); and half-stick, three-fourths–stick, and full-stick rolls. Push-over–pull-up maneuvers designed for nose-boom air data calibration also were flown. Figure 4 presents the flight conditions at which these maneuvers were flown.

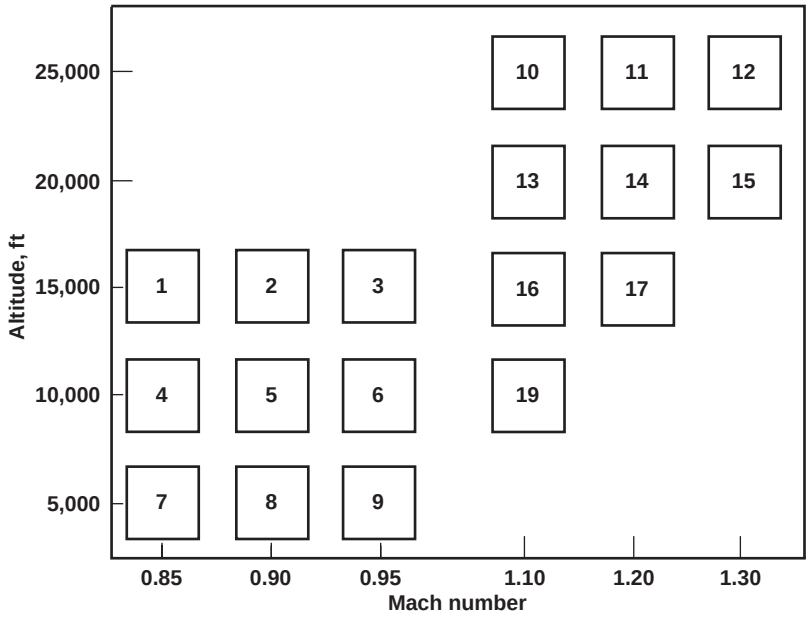

Figure 4. Active Aeroelastic Wing flight conditions.

III. Data Conditioning

Several data conditioning steps were performed before the data could be used to create a loads model. Considerable emphasis was placed on data conditioning because of concern that data spikes, noisy data, or invalid data could cause the loads model to improperly characterize cause and effect relationships. The initial steps involved filling in data dropouts and missing data points by means of linear interpolation. This step was performed to prevent distortions caused by filtering. The data then were synchronized in time through the use of time signals correlated with each data source on the airplane. Data spikes then were removed with an interactive spike removal tool, and the data were filtered with fifth-order low-pass Butterworth filters. Cutoff frequencies for these filters were approximately one-half of the lowest aircraft structural mode frequency. The filters were run forward and backward to eliminate filter-induced phase lag. After filtering, the data points were resampled at the sample rate of the surface positions through the use of linear interpolation. The next step involved the removal of any data points that were added by interpolation during the previous steps. Interpolated data were removed, because they were added for filtering only. After the inserted data points were removed, each input parameter was scaled using preset scale factors. Scale factors were chosen from simulated roll maneuvers to normalize the inputs to an approximate range of ±1.0. When scaled parameters are used, the importance of an input in the model can be judged by the value of its corresponding model coefficient.

Separate data sets were used to define the aircraft states and control surface positions associated with the left and right wing loads. When symmetry is assumed, both left and right wing loads can be used to derive a single load equation. This derivation was accomplished by reversing the sign on the lateral-directional states and differential surface positions for left-wing data sets. To de-emphasize loads at trim, specific sections of data were resampled at a lower sample rate to adjust data density during each maneuver when the load was low. Because the number of data points was reduced at low loads, high load data were given more priority by the regression process.

IV. Loads Model Development

The AAW loads model is a collection of load equations in which each equation defines a single component load at a single flight condition. The component loads that were modeled for the AAW are wing-root bending moment (WRBM), wing-root torque (WRTQ), wing-fold bending moment (WFBM), wing-fold torque (WFTQ), inboard leading-edge flap hinge moment (ILEF HM), outboard leading-edge flap hinge moment (OLEF HM), trailing-edge flap hinge moment (TEF HM), and aileron hinge moment (Ail HM). The form of each load equation is shown in Eq. (1).

$$L_{pred} = I + \sum_{j=1}^{R} A_j X_j \tag{1}$$

The term L_{pred} is the predicted load from the loads model, I is the intercept term, R is the number of inputs, and X is the set of input parameters used in each load equation. The equation coefficients, A, were derived using multiple linear regression. The intercept term, I, was allowed to differ for left and right load equations to account for measurement biases and aircraft asymmetry. Multiple linear regression produces equation coefficients that minimize the sum of the squared errors as shown in Eq. (2),

$$Err_{sumsq} = \sum_{i=1}^{N} \left(L_{meas_i} - L_{pred_i} \right)^2 \tag{2}$$

where L_{meas} is the measured load and N is the number of data samples. The equation coefficients can be obtained directly using matrix inversion, as shown in Eq. (3).[11]

$$A = \left[X^T X \right]^{-1} X^T L_{meas} \tag{3}$$

The input set, X, was chosen for each load equation from a set of aircraft states and control surface positions. The AAW loads model primarily was intended as a control law design tool used with a simulation of the AAW aircraft. Therefore, only parameters that were available in the simulation were used as inputs to the loads model. For this reason, surface actuator positions were used instead of measured surface positions. The measured surface positions differ from the surface actuator positions because of surface flexibility. Table 3 presents the set of all candidate aircraft states and surface actuator positions used for model development. Table 4 lists the new input variables that were calculated from the parameters provided in table 3. These new input variables were created to account for nonlinear load responses. Generally, the calculated parameters only slightly improved the accuracy of the model. Inputs were chosen for each load equation from the set provided in tables 3 and 4. The determination of an input set for each load equation involved several steps. First, all possible input combinations were examined to find a subset of inputs that produced the lowest error shown in Eq. (2). The input set that was chosen was further refined by disallowing highly correlated inputs, such as normal acceleration and angle of attack, in the same load equation.

Table 3. Measured inputs.

Parameter	Description
Mach	Mach number
$\bar{q}$	Dynamic pressure
α	Angle of attack
β	Angle of sideslip
p	Roll rate
Nz	Normal acceleration
$ILEF_L$	Left inboard leading-edge flap position
$ILEF_R$	Right inboard leading-edge flap position
$OLEF_L$	Left outboard leading-edge flap position
$OLEF_R$	Right outboard leading-edge flap position
TEF_L	Left trailing-edge flap position
TEF_R	Right trailing-edge flap position
Ail_L	Left aileron position
Ail_R	Right aileron position

Table 4. Calculated inputs.

Parameter	Equation
NzW	Nz(total aircraft weight)
Ail_sq	sign(Ail)(Ail)^2
TEF_pos	$\begin{cases} 0 & \text{for TEF} > 0 \\ \text{TEF} & \text{for TEF} \geq 0 \end{cases}$
$ILEF_C$	$.5(ILEF_L + ILEF_R)$
$ILEF_D$	$ILEF_R - ILEF_L$
$OLEF_C$	$.5(OLEF_L + OLEF_R)$
$OLEF_D$	$OLEF_R - OLEF_L$
Ail_C	$.5(Ail_L + Ail_R)$
Ail_D	$Ail_L - Ail_R$
TEF_C	$.5(TEF_L + TEF_R)$
TEF_D	$TEF_L - TEF_R$
$Stab_C$	$.5(Stab_L + Stab_R)$

Phase 1 flight data were used to derive the equation coefficients and assess model accuracy. Phase 1 maneuvers consisted of OBES maneuvers and piloted maneuvers. The OBES maneuvers primarily were used to derive equation coefficients, whereas piloted maneuvers were used for both validation and derivation. Piloted maneuvers consisted of rolls, 5-*g* WUTs, 4-*g* RPOs, and push-over–pull-up maneuvers. A typical set of derivation maneuvers consisted of small, medium, and large collective and differential OBES maneuvers, a WUT, a half-stick roll, a full-stick roll, and a full-stick RPO. Validation with independent maneuvers was an important step in the development of the loads model. This step allowed the user to check the model for hidden problems, such as highly correlated inputs and

misidentified input-to-load relationships, which would not have been found by only comparing model accuracy to derivation maneuvers. A typical set of validation maneuvers consisted of a medium collective OBES maneuver, medium differential OBES maneuver, three-fourths–stick roll, WUT, and three-fourths–stick RPO. The quality of the loads model was determined with the load prediction error shown in Eq. (4). This error calculation is hereafter used in this report to show the performance of the loads model. The load prediction errors for phase 1 maneuvers ranged from 2 to 20 percent and typically were slightly better for derivation maneuvers than for validation maneuvers.

$$Err_{model} = \frac{\sqrt{\sum_{i=1}^{N}\left(L_{meas_i} - L_{pred_i}\right)^2}}{\text{load limit}} \tag{4}$$

The loads model was implemented in the nonlinear simulation for control law design and testing purposes. The AAW phase 2 control law design process interfaced with the simulator and attempted to maximize roll performance while maintaining loads within boundaries and providing adequate handling qualities.[2] Because the optimization process tended to push at least one wing load or surface hinge moment to its limit, additional margins were placed on the load limits to account for loads model prediction uncertainty. Loads model uncertainty at limit loads could not be obtained directly, because the flight data did not always include high-load data for each load. In these cases, uncertainty was estimated from cross plots of measured load as a function of predicted load and scatter plots of model prediction error as a function of measured load. Figures 5 and 6 show a typical set of these plots. Figure 5 shows trends in the loads model prediction as the load increases. These trends were useful in estimating the amount of loads model over-prediction or under-prediction that could occur at high load values. Figure 6 shows the load prediction error as a function of measured load. Positive errors on this plot indicate loads model over-prediction. From these two plots, uncertainty bounds of 10 percent for negative limit loads and five percent for positive limit loads were used for this load in control design. These relatively low values were used, because the trends seen in Figs. 5 and 6 show that high loads will be over-predicted by the model and thus are conservative. The loads model over-prediction of high loads and under-prediction of low loads was a typical occurrence for the control surface hinge moments.

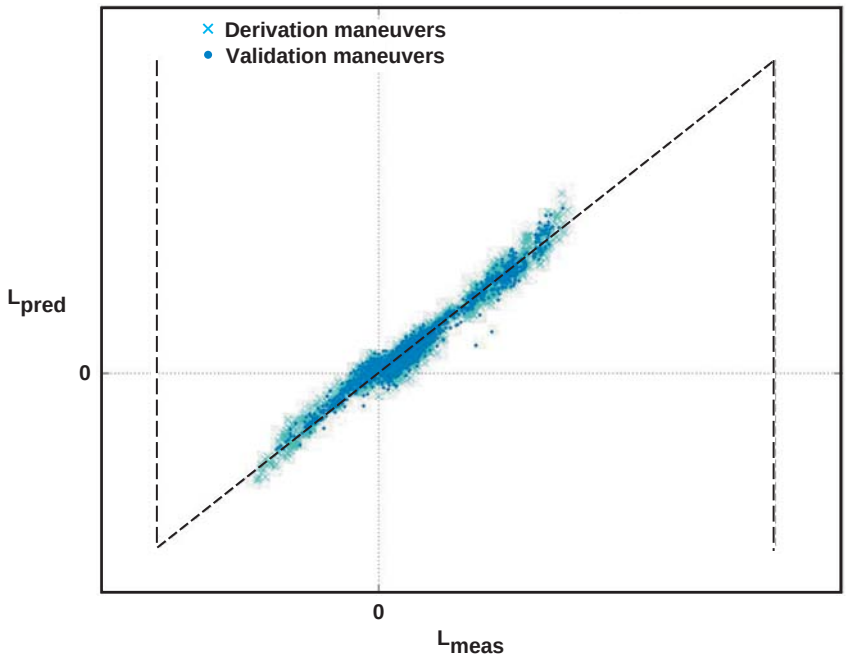

Figure 5. Load prediction cross plot of the inboard leading-edge flap hinge moment at Mach 0.90, 5,000-ft altitude (flight condition 8).

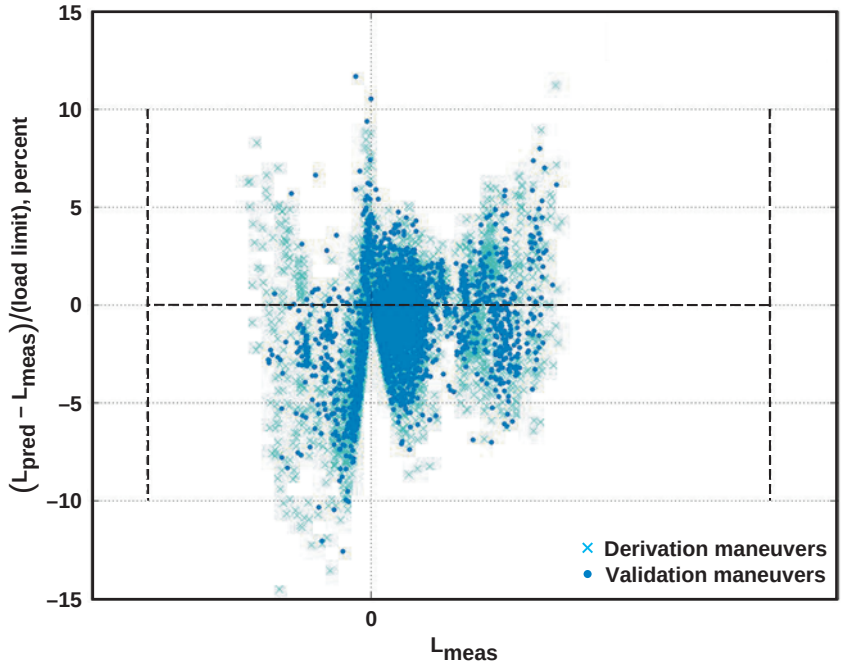

Figure 6. Load prediction error as a function of measured inboard leading-edge flap hinge moment at Mach 0.90, 5,000-ft altitude (flight condition 8).

V. Phase 2 Results

Phase 2 of the AAW project was used to evaluate the use of wing twist for roll control. New control laws[2] were designed at the NASA Dryden Flight Research Center (Edwards, California) through the use of the loads model described in this report. During the spring of 2005, these control laws were flown with the AAW aircraft and subsequently analyzed. Load time histories and load prediction error tables for these maneuvers are presented in this section to demonstrate the final accuracy of the loads model during its intended use. Many of the phase 2 maneuvers cause the leading-edge flap hinge moment equations to significantly extrapolate from the phase 1 data used to create the model. The lack of sufficient phase 1 data used for these loads was a result of small magnitude leading-edge flap OBES maneuvers and the limited use of leading-edge flaps by the standard F/A-18 control system at the AAW flight conditions. The OBES maneuvers were a smaller fraction of the limit load than desired, because the original analytically derived loads model significantly over-predicted the leading-edge flap hinge moments.[3]

Figure 7 shows a typical time history plot for the leading-edge flap hinge moments during a full-stick roll. This plot shows the over-prediction of the leading-edge flap hinge moments by the loads model. Figure 8 shows the shape of the loads model prediction as load increases. A perfect load prediction would follow the dashed line in Fig. 8, indicating that the predicted load was equal to the measured load. Loads model errors caused by time skew in the load prediction were removed from this plot. The overall nonlinear trend in the measured leading-edge flap hinge moments seen in this plot was only approximated by the prediction. Sources of nonlinearity include control surface free play, control surface flexibility, Mach effects, and partial flow separation. Table 5 lists the model prediction errors for the left and right leading-edge flap hinge moments during maximum-stick rolls at all of the AAW flight conditions. Errors that are greater than 20 percent are shaded in the table to indicate poor load predictions. Figure 9 shows the TEF and aileron hinge moments during the same maneuver as that presented in Fig. 7. This figure shows good load predictions by the loads model. The difference in accuracy for leading-edge load predictions and trailing-edge load predictions is partially caused by the size of the phase 1 input maneuvers used to derive the loads model. Small inputs were used for the leading-edge flap excitation maneuvers, whereas large inputs were used for the TEF and aileron excitation maneuvers. The limited input size of the leading-edge flap maneuvers caused degradation in leading-edge flap hinge moment prediction accuracy. Fortunately, this degradation usually did not affect the control law design, because the leading-edge flap positions often were limited by other constraints.

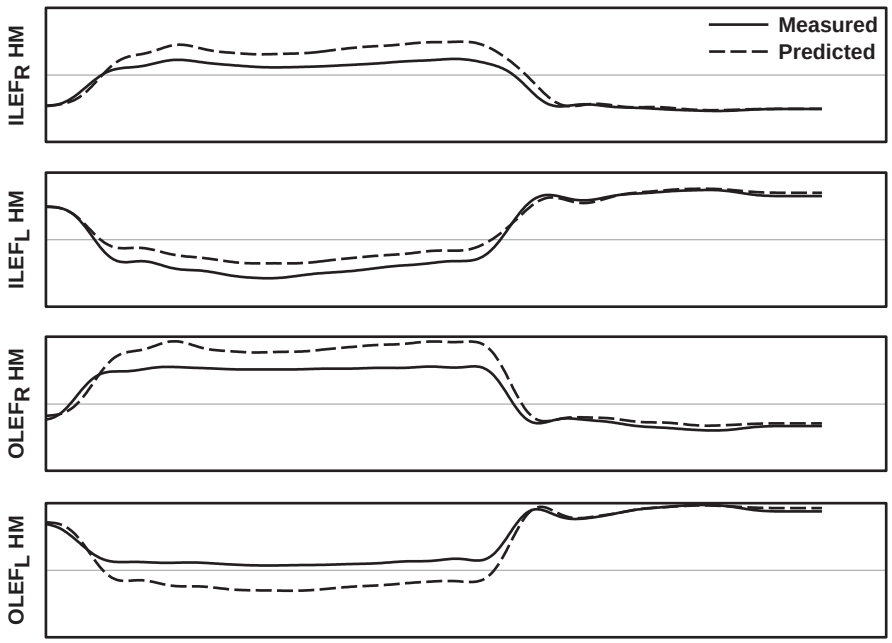

Figure 7. Leading-edge flap hinge moments during a full-stick roll at Mach 1.1, 20,000-ft altitude (flight condition 13).

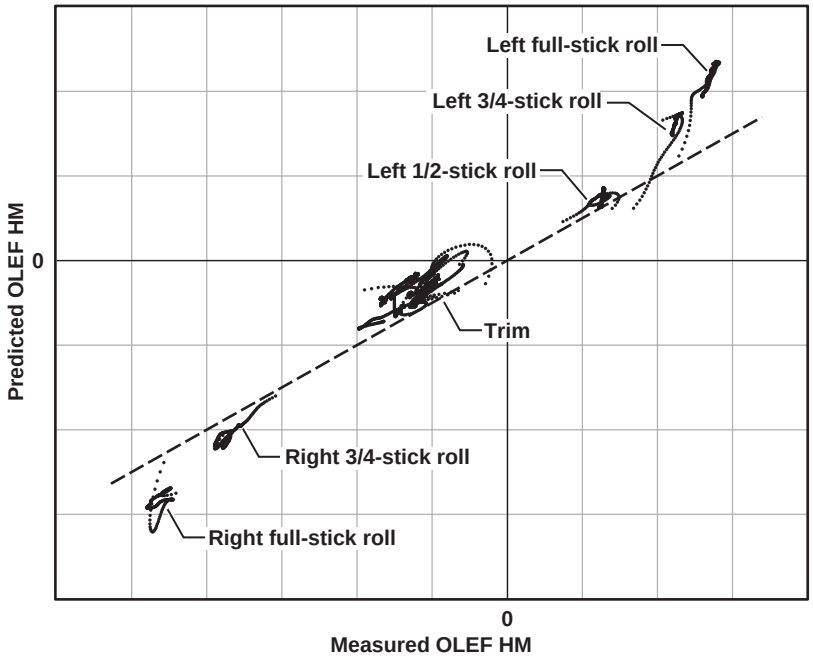

Figure 8. Scatter plot of predicted outboard leading-edge flap hinge moment (OLEF HM) as a function of measured OLEF HM during roll maneuvers at Mach 1.1, 20,000-ft altitude (flight condition 13).

Table 5. Model prediction errors for the leading-edge-flap hinge moments during maximum-stick rolls at all flight conditions.

Mach number	Altitude, ft	$ILEF_R$ HM	$ILEF_L$ HM	$OLEF_R$ HM	$OLEF_L$ HM
0.85	15,000	5.7	2.8	9.0	11.7
0.90	15,000	4.1	5.7	15.3	16.5
0.95	15,000	6.4	2.5	11.7	27.6
0.85	10,000	4.0	6.0	10.1	1.9
0.90	10,000	10.1	5.5	19.4	10.1
0.95	10,000	1.7	1.3	4.4	29.0
0.85	5,000	6.7	6.3	3.2	4.0
0.90	5,000	12.0	10.6	16.6	14.5
0.95	5,000	7.4	3.5	26.7	17.1
1.10	25,000	4.5	8.6	2.6	6.2
1.20	25,000	7.3	7.7	18.5	5.4
1.30	25,000	3.9	8.3	8.2	11.4
1.10	20,000	6.4	7.5	18.8	20.2
1.20	20,000	8.0	12.7	12.8	10.1
1.30	20,000	11.7	27.7	7.0	14.0
1.10	15,000	10.4	14.4	10.6	2.4
1.20	15,000	12.7	22.5	21.5	13.4
1.10	10,000	8.8	29.6	11.0	16.7

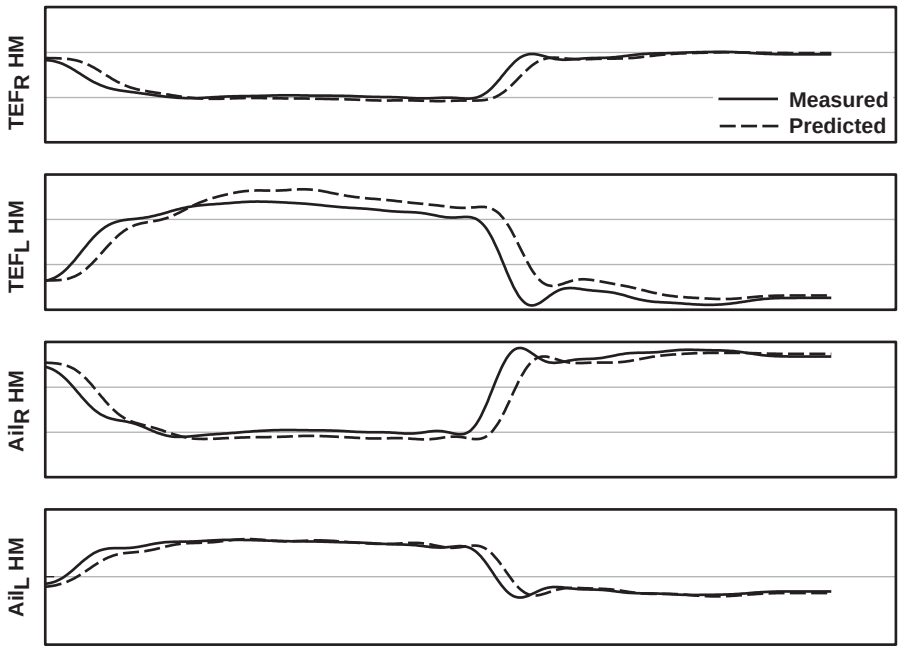

Figure 9. Trailing-edge flap and aileron hinge moments during a full-stick roll at Mach 1.1, 20,000-ft altitude (flight condition 13).

Windup-turn maneuvers flown to 5-*g* normal acceleration also were used in the phase 2 flight test for envelope expansion, aerodynamic model validation, and loads model validation. These maneuvers caused much higher wing-root and wing-fold bending moment loads than the roll maneuvers. Figure 10 shows typical time history plots of the WRBM, WFBM, WRTQ, and WFTQ loads of the left wing. Bending moment predictions provided by the loads model have lower model prediction errors than the torque predictions. This decrease likely is a result of the smaller magnitude of the torque response. The small jump in the measured WFTQ that occurs 4 seconds into the maneuver is caused by free play in the OLEF.

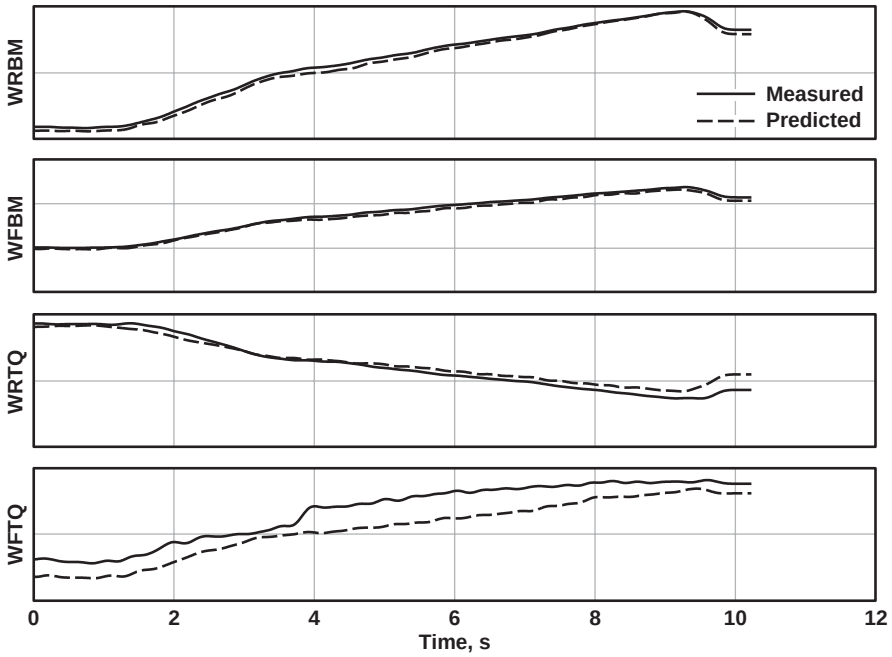

Figure 10. Typical bending and torque loads during a 5-*g* windup turn.

Tables 6 and 7 present the overall performance of the loads model. These tables show the model prediction errors, calculated from Eq. (5), for various maneuvers. The maximum roll maneuver shown in these tables is the largest maneuver from the set of roll buildup maneuvers flown in phase 2. The maximum roll maneuver often was a full-stick roll, but the roll buildup occasionally was halted at a lower stick deflection for safety reasons. The roll errors indicate the performance of the loads model during its intended use as a control law design tool for a roll control experiment. These errors are generally low, indicating a good match between flight-measured load and model-predicted load. The highest error occurs in the prediction of the OLEF HM. These loads were consistently over-predicted by the loads model, as described previously. The average load prediction error across all flight conditions for the maximum roll maneuver is 9.1 percent.

Table 6. Average subsonic model prediction root-mean-square errors.

Load	Maximum rolls, percent	5-*g* WUT, percent	4-*g* RPO, percent
WRBM	10.1	2.8	4.6
WRTQ	5.3	4.4	7.8
WFBM	6.1	2.6	5.9
WFTQ	9.9	6.7	15.1
ILEF HM	5.5	4.6	7.9
OLEF HM	15.7	11.8	14.4
TEF HM	6.1	3.8	7.4
Ail HM	10.6	4.9	12.0
Mean	8.7	5.2	9.4

Table 7. Average supersonic model prediction root-mean-square errors.

Load	Maximum rolls, percent	5-*g* WUT, percent	4-*g* RPO, percent
WRBM	13.9	1.4	4.9
WRTQ	5.9	3.0	3.7
WFBM	7.5	1.8	4.4
WFTQ	5.2	3.6	6.3
ILEF HM	12.3	2.5	4.7
OLEF HM	13.0	8.7	11.5
TEF HM	7.2	3.8	5.1
Ail HM	10.1	4.2	7.4
Mean	9.4	3.6	6.0

The loads model prediction of WUT loads generally was good. The lowest error for these maneuvers is 1.4 percent for the WRBM. The highest error is 11.8 percent for the OLEF HM. The loads during 5-*g* WUTs generally were the easiest to model. The average load prediction error across all flight conditions for the WUTs is 4.4 percent.

The RPO maneuvers were used to test the combination of longitudinal and lateral maneuvering on the aircraft. A single RPO maneuver consists of a 4-*g* WUT combined with roll input. Loads resulting from RPO maneuvers typically were the most difficult to predict. The RPOs were flown at every flight condition except Mach 1.1 and an altitude of 10,000 ft. The average load prediction error for all RPO maneuvers is 7.7 percent. Load prediction errors during these maneuvers may result from the lack of superposition in the aircraft load response. The loads model assumes that superposition is valid for this application. In reality, combined longitudinal and lateral maneuvering may cause an aircraft loading that is different from a simple sum of longitudinal and lateral inputs. Average supersonic load predictions are consistently better for all maneuvers. This trend is consistent with model development and analysis with phase 1 flight data. This trend may be caused by the reduction of transonic shock-effects that occur at subsonic flight conditions.

VI. Summary of Results

A loads model for the design and analysis of new control laws for the Active Aeroelastic Wing airplane was successfully completed using multiple linear regression of flight data. Analysis of the loads model with flight data through the use of the new control laws provided the following results:

1) The use of surface doublet maneuvers, rolls, 5-*g* windup turns, and 4-*g* rolling pullouts worked effectively to create a loads model for the Active Aeroelastic Wing control law design.
2) The use of separate maneuvers to validate the loads model was useful during loads model development to ensure that potential problems were identified.
3) The load prediction errors for phase 1 maneuvers ranged from 2 to 20 percent and typically were slightly better for derivation maneuvers than for validation maneuvers.
4) Insufficient excitation of the leading-edge flap hinge moments and nonlinear load responses in the model development data caused degradation of loads model prediction accuracy for those loads.
5) The loads model generally predicted loads more accurately during 5-*g* windup turns than during rolls or rolling pullouts.
6) The loads model generally predicted loads from rolling pullout maneuvers less accurately than loads from other maneuvers.
7) The loads model accurately predicted loads caused by roll maneuvers, with the exception of the leading-edge flap hinge moments at some flight conditions.
8) The average load prediction errors for all loads at all flight conditions were 9.1 percent for maximum stick-deflection rolls, 4.4 percent for 5-*g* windup turns, and 7.7 percent for 4-*g* rolling pullouts.
9) Overall, good load prediction was obtained for subsonic and supersonic wing-root and wing-fold bending moments and torque loads, in addition to trailing-edge control surface hinge moments.

References

[1]Pendleton, E., Bessette, D., Field, P., Miller, G., and Griffin, K., "The Active Aeroelastic Wing Flight Research Program Technical Program & Model Analytical Development," AIAA-98-1972, 1998.

[2]Dibley, R., Allen, M. J., Clarke, R., Gera, J., and Hodgkinson, J., "Development and Testing of Control Laws for the Active Aeroelastic Wing Program," AIAA-2005-6134, to be presented at the *AIAA Atmospheric Flight Mechanics Conference and Exhibit*, San Francisco, CA, August 15–18, 2005.

[3]Olney, C. D., Hillebrandt, H., and Reichenbach, E. Y., "An Evaluation Technique for an F/A-18 Aircraft Loads Model Using F/A-18 Systems Research Aircraft Flight Data," NASA TM-2000-209028, 2000.

[4]Lewis, G. E., "AFTI/F-111 Mission Adaptive Wing Maneuver Load Control," available from the NASA Center for AeroSpace Information (CASI), CASI document identification 19910074478.

[5]Haas, D. J., Flitter, L., and Milano, J., "Helicopter Flight Data Feature Extraction or Component Load Monitoring," *Journal of Aircraft*, Vol. 33, No. 1, Jan.–Feb. 1996.

[6]Haas, D. J., and Imber, R., "Identification of Helicopter Component Loads Using Multiple Regression," *Journal of Aircraft*, Vol. 31, No. 4, July–Aug. 1994.

[7]Haas, D. J., Milano, J., and Flitter, L., "Prediction of Helicopter Component Loads Using Neural Networks," *Journal of the American Helicopter Society*, Vol. 40, No. 1, Jan. 1995.

[8]Allen, M. J., and Dibley, R. P., "Modeling Aircraft Wing Loads from Flight Data Using Neural Networks," NASA/TM-2003-212032, 2003.

[9]Lokos, W. A., Olney, C. D., Chen, T., Crawford, N. D., Stauf, R., and Reichenbach, E. Y., "Strain-Gage Loads Calibration Testing of the Active Aeroelastic Wing F/A-18 Airplane," AIAA 2002-2926, 2002.

[10]Lokos, W. A., and Stauf, R., "Strain-Gage Loads Calibration Parametric Study," NASA TM-2004-212853, 2004.

[11]Chapra, S. C., and Canale, R. P., *Numerical Methods for Engineers*, 2nd ed., McGraw-Hill, Inc., New York, St. Louis, San Francisco, 1988.